REPORT DOCUMENTATION PAGE

AFRL-SR-AR-TR-05-
0046

Public reporting burden for this collection of information is estimated to average 1 hour per response, including the gathering and maintaining the data needed, and completing and reviewing the collection of information. Send cor collection of information, including suggestions for reducing this burden, to Washington Headquarters Services, Di Davis Highway, Suite 1204, Arlington, VA 22202-4302, and to the Office of Management and Budget, Paperwork

1. AGENCY USE ONLY *(Leave blank)*	2. REPORT DATE	3. REPORT TYPE AND DATES COVERED
		01 Jun 2001 - 31 Dec 2004 FINAL

4. TITLE AND SUBTITLE
Systematic Studies of Carbon Doping in High Quality GaN Growth by Molecular Beam Epitaxy

5. FUNDING NUMBERS
61102F
2305/BX

6. AUTHOR(S)
Professor Speck

7. PERFORMING ORGANIZATION NAME(S) AND ADDRESS(ES)
UNIVERSITY OF CALIFORNIA
CHEADLE HALL
SANTA BARBARA CA 93106-2050

8. PERFORMING ORGANIZATION REPORT NUMBER

9. SPONSORING/MONITORING AGENCY NAME(S) AND ADDRESS(ES)
AFOSR/NE
4015 WILSON BLVD
SUITE 713
ARLINGTON VA 22203

10. SPONSORING/MONITORING AGENCY REPORT NUMBER
F49620-01-1-0314

11. SUPPLEMENTARY NOTES

12a. DISTRIBUTION AVAILABILITY STATEMENT
DISTRIBUTION STATEMENT A: Unlimited

DISTRIBUTION STATEMENT A
Approved for Public Release
Distribution Unlimited

12b. DISTRIBUTION CODE

13. ABSTRACT *(Maximum 200 words)*
For the final contract period September 1, 2003 — December 31, 2004, we have completed the following tasks:

- Successfully incorporated carbon into all MBE-grown HEMTs (in conjunction with the DARPA Wide Bandgap Semiconductor program) and realized record power non-field- plated GaN HEMTs (for both MBE and MOCVD.
- In collaboration with Prof Steve Ringel's group at Ohio State (under ON7R support), completed an initial study of deep level optical studies of carbon-doped MBE GaN.
- Completed initial studies of Fe-doping in MBE GaN as an alternative approach for realizing semi-insulating GaN.

14. SUBJECT TERMS

15. NUMBER OF PAGES

16. PRICE CODE

17. SECURITY CLASSIFICATION OF REPORT	18. SECURITY CLASSIFICATION OF THIS PAGE	19. SECURITY CLASSIFICATION OF ABSTRACT	20. LIMITATION OF ABSTRACT
Unclassified	Unclassified	Unclassified	UL

Standard Form 298 (Rev. 2-89) (EG)
Prescribed by ANSI Std. 239.18
Designed using Perform Pro, WHS/DIOR, Oct 94

A ~~Progress~~ Final Report to

The Air Force Office of Scientific Research

Program Manager:

Dr. Gerald L. Witt
AFOSR/NE
801 N. Randolph St., Rm 732
Arlington, VA 22203
VOICE: (703) 696-8571

Systematic Studies of Carbon Doping in High Quality GaN Grown by Molecular Beam Epitaxy

AFOSR Award # F49620-01-1-0314

September 1, 2003 – December 31, 2004

James S. Speck
Materials Department
University of California
Santa Barbara, CA 93106

DISTRIBUTION STATEMENT A
Approved for Public Release
Distribution Unlimited

20050218 050

Introduction

This AFOSR program is focused on the behavior of common impurities in GaN and its alloys and specifically focused on the behavior of carbon. In MOCVD-grown GaN, the most common unintentional impurities are oxygen, hydrogen, and carbon. It is clear from numerous experiments and from theory that oxygen is a shallow donor in GaN and in $x < \sim 0.35$ Al-content $Al_xGa_{1-x}N$. For higher Al content $Al_xGa_{1-x}N$, oxygen has DX behavior and becomes a deep acceptor. The behavior of hydrogen in GaN is not fully understood. However, it is clear that hydrogen forms complexes with magnesium and passivates magnesium acceptors. The behavior of carbon in GaN has also been elusive and its energy levels in GaN remain unresolved. Carbon produces shallow acceptor states in GaAs, GaP, and InP, however its role in GaN is poorly understood. Experimental results have shown carbon to be a shallow acceptor, a donor, and a deep level compensating center as well as a self-compensator. These seemingly conflicting results are due to the amphoteric nature of carbon and the different growth conditions used in each study.

The present program is focused on doping GaN using a CBr_4 injector in an ultra high purity molecular beam epitaxy (MBE) system capable of growing high quality, low impurity GaN films. In this program, we have now successfully incorporated carbon into MBE-grown GaN via CBr_4, realized semi-insulating buffer layers in HEMT structures via carbon doping, and determined the energy levels for carbon in GaN.

In this final contract period (in part under a no-cost extension), we have nearly completed our basic studies on carbon in GaN; we have also completed preliminary studies of Fe-doping of GaN by rf-plasma-assisted MBE.

Technical Goals

For the final contract period September 1, 2003 – December 31, 2004, we have completed the following tasks:

- Successfully incorporated carbon into all MBE-grown HEMTs (in conjunction with the DARPA Wide Bandgap Semiconductor program) and realized record power non-field-plated GaN HEMTs (for both MBE and MOCVD.
- In collaboration with Prof. Steve Ringel's group at Ohio State (under ONR support), completed an initial study of deep level optical studies of carbon-doped MBE GaN.
- Completed initial studies of Fe-doping in MBE GaN as an alternative approach for realizing semi-insulating GaN.

We summarize these results below.

detectable Br incorporation into the GaN, no other measurable change in incorporation of other unintentional impurities (e.g., oxygen). Our initial efforts to produce all MBE-grown GaN-based HEMTs were plagued by problems associated with buffer leakage. Our early carbon-free HEMTs were limited to powers of ~ 4W/mm with only ~19% PAE at 10 GHz.. Carbon doping solved our buffer leakage issues and improved our HEMT performance to 6.6 W/mm with 57% PAE at 4 GHz and 7.3 W/mm with 36% PAE at 10 GHz.

In the current reporting period, we have continued to optimize the all MBE-grown HEMT. By continuing to use carbon doping in the first 400 nm of the GaN buffer on AlN on SiC, we have realized powers as high as 12 W/mm with 46% PAE at 4 GHZ on non-field-plated devices, as shown in Fig. 1 – these are the highest powers for non-field-plated HEMTs (later this value was realized by MOCVD UCSB for GaN-based HEMTs with thick GaN caps). Our initial efforts at field-plated results were also successful. The first field-plated devices had powers as high as 15 W/mm with 55% PAE at 4GHz, as shown in Fig. 2.

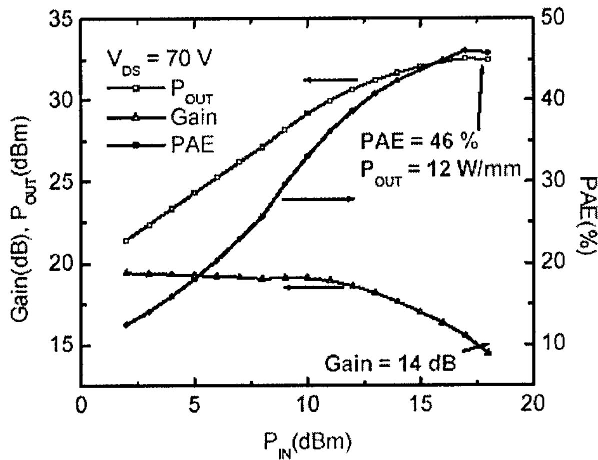

Figure 1 Transistor characteristics of a non-field-plated all MBE GaN-based HEMT measured at 4GHz. This structure concisted of 30 nm $Al_{0.30}Ga_{0.70}N$ / 1 μm UID GaN / 0.4 μm GaN:C / 45 nm AlN / SiC.

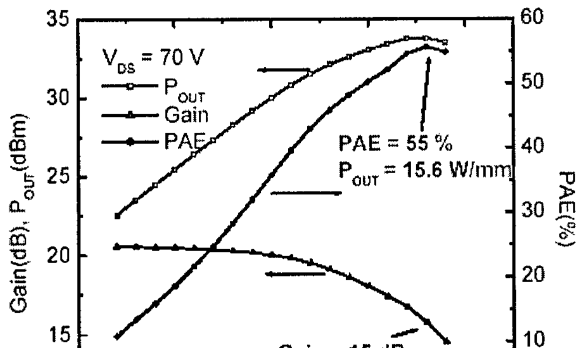

Figure 2 Transistor characteristics of a field-plated all MBE GaN-based HEMT measured at 4GHz. This structure concisted of 30 nm $Al_{0.30}Ga_{0.70}N$ / 1 μm UID GaN / 0.4 μm GaN:C / 45 nm AlN / SiC. .

Deep level optical spectroscopy studies of carbon in MBE GaN

We have continued to work closely with Prof. Steve Ringel's group on deep level optical spectroscopy (DLOS) studies of GaN. During the time of the current program, we have provided Prof. Ringel's group with n-type GaN samples co-doped with carbon, i.e., GaN:Si:C for DLOS studies. These samples were specifically grown for Ringel's group.

Our work on carbon in GaN continues to be guided by the theoretical work on the role of carbon in GaN has been performed by A.F. Wright and co-workers at Sandia National Laboratories. In a seminal paper on carbon in GaN [C.H. Seager *et al, J. Appl. Phys.* **92** (2002)], electronic structure calculations by Wright showed that carbon in GaN should show amphoteric behavior and also the incorporation energetics of the carbon depends on the GaN growth conditions. The main results, summarized below in Fig. 3, are as follows: carbon on the nitrogen site is a shallow acceptor (favored for carbon in n-type GaN); carbon on the Ga site is a shallow donor (favored for carbon in p-type GaN); and carbon may also occupy interstitial sites – the charge behavior for interstitial carbon is more complicated.

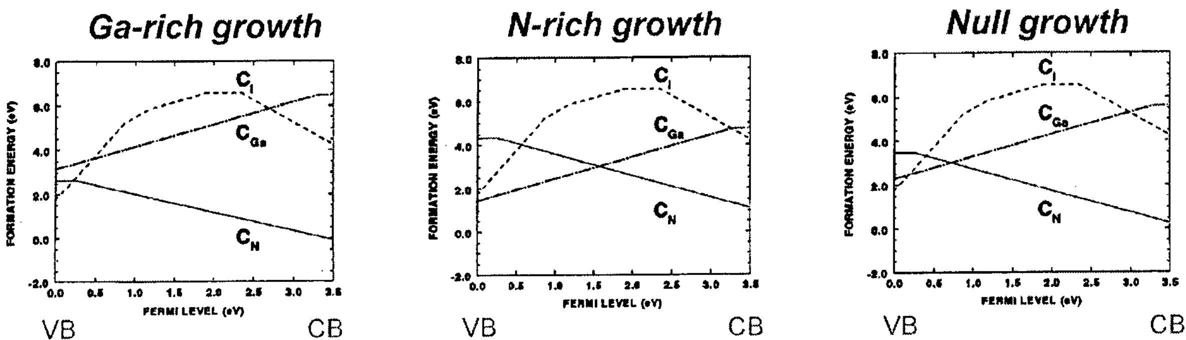

Figure 3 Calculations of the Fermi-level dependence of the formation energy of carbon on the nitrogen site (C_N), gallium site (C_{Ga}), and interstitial sites (C_I)in GaN (from C.H. Seager *et al., J. Appl. Phys.* **92** (2002)).

The key results on the GaN:Si:C samples are shown in Fig. 4. The E_c – 3.28 eV level is the shallow carbon acceptor predicted to be stable in n-type GaN. The E_c – 1.94 eV level appears to be associated with interstitial carbon C_I – these levels appear to verify the main predictions of Wright and co-workers.

Ringel's group has also developed a new an exciting model for yellow luminescence (YL) in GaN. In the GaN:Si:C series sent to OSU, samples without carbon were *n*-type and demonstrated a weak yellow luminescence band, likely related to V_{Ga}. For increasing carbon co-doping, samples became semi-insulating concurrent with increased intensity of the yellow luminescence and the concentration of C-related deep acceptors. The DLOS results were used to develop a configuration-coordinate model for a C-related deep level with optical ionization

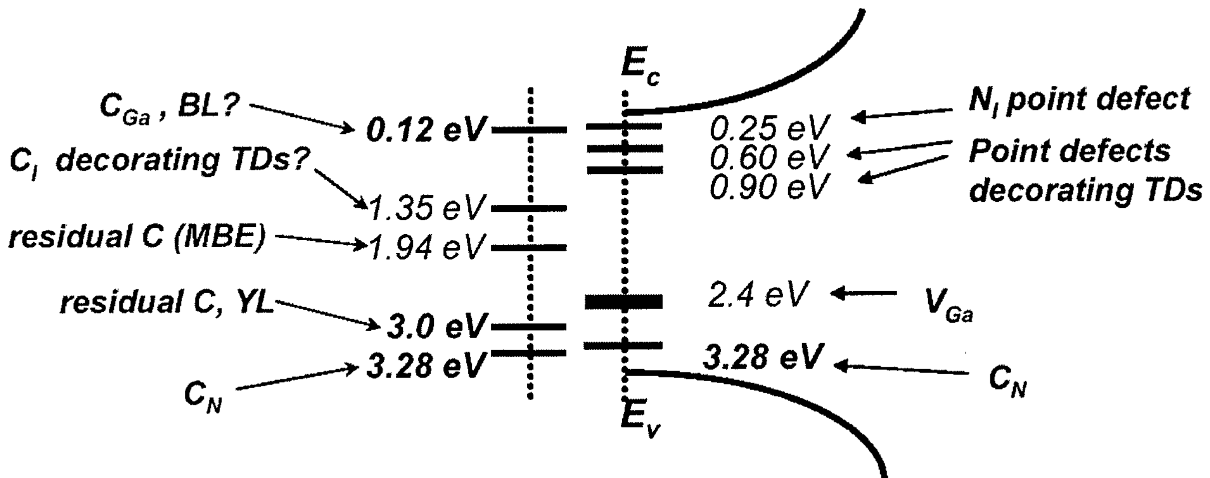

Figure 4 Summary of key findings of DLOS studies of carbon in n-type MBE GaN (in collaboration with Prof. Steve Ringel's group at Ohio State). The states on the left are associated with carbon (in **blue**) in n-type MBE GaN. The states on the right (**red**) are typically observed in n-type MBE GaN (no intentional carbon doping). The E_c – 3.28 eV and E_c – 1.94 eV carbon-related levels appear to verify the theoretical models of Wright.

Studies of iron incorporation in MBE GaN

The success of Fe-doping in producing semi-insulating MOCVD GaN has lead to its widespread use in device structures, and Fe-doped semi-insulating GaN templates are now commercially available. In addition to transition-metal doping GaN in order to achieve semi-insulating material, there is widespread interest in this topic within the field of spintronics. However, very little work has been done on Fe-doping GaN films by MBE. The few papers that do exist in the literature on MBE-grown Fe-doped GaN primarily focus on magnetic properties of the films, with little/no attention paid to electrical or structural properties (see: S. Kuwabara *et al.*, *Jpn. J. Appl. Phys.* **40**, L724 (2001); H. Ofuchi et al., *Appl. Phys. Lett.* **78**, 2470 (2001); and H. Akinaga *et al.*, *Appl. Phys. Lett.* **77**, 4377 (2000)). In this work, we grew MBE-grown Fe-doped GaN films and characterized their structural and electrical properties in order to achieve semi-insulating material and better understand this system.

Approach: Nominally Fe-doped GaN films were grown by MBE using an rf plasma N_2 source and a high-purity solid Fe source on MOCVD GaN/sapphire templates purchased from Lumilog (Vallauris, France). The samples were grown at a nominal temperature of 650 °C as determined by a high-temperature pyrometer, and were grown in various regions of the GaN MBE growth diagram: Ga-droplet, intermediate, and N-rich. Fe cell temperatures varied from 840 °C to 1000 °C; at these temperatures, the flux from the cell was too low to be accurately

were polished manually and imaged on an FEI T20 microscope at 200 kV under two-beam bright-field conditions for various g vectors. AFM was performed in tapping mode on a Digital Instruments Dimension 3100 microscope. For CV measurements, thin (~130 nm) N-rich Fe-doped films were grown on n-type Si-doped GaN templates, patterned, and etched down to the n-type template in order to define Fe-doped GaN mesas. Ti/Al/Ni/Au contacts were made to the n-type template material and the Fe-doped mesas, and CV measurements were performed on an Agilent 4294A impedance analyzer with frequency range 40 Hz – 110 MHz.

Findings: Typical SIMS data for a sample grown in the Ga-droplet regime with an Fe cell temperature of 1000° C is shown in Fig. 5, along with a schematic of the sample structure. The Fe signal peaks toward the surface of the sample, and quickly decreases to the background level, with no appreciable Fe incorporation in the nominally Fe-doped layer. Fig. 6 shows a corresponding Fe^{+} ion image recorded by SIMS at a crater depth of approximately 100 nm, and an AFM image of the same scale with Ga droplets highlighted in yellow.

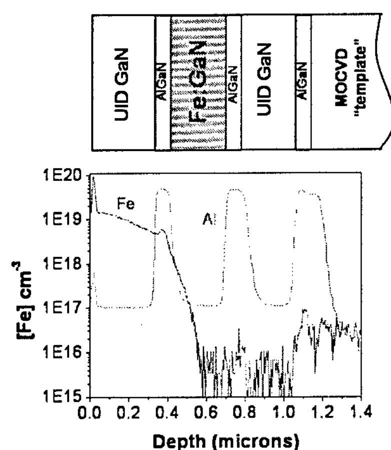

Figure 5 SIMS data and schematic of a nominally Fe-doped sample grown in the Ga-droplet growth regime.

Figure 6 SIMS Fe^{+} image showing localized areas of high Fe concentration in yellow (top) and AFM image with Ga droplets highlighted (bottom).

The similarity in size and distribution of Ga droplets in the AFM image and the yellow Fe-rich areas in the SIMS image suggests that these Fe-rich regions are associated with droplets. The surface imaged in AFM was typical of UID GaN grown in this regime: it was smooth and free of anomalous features. Additional samples were grown in the Ga droplet regime for various Fe fluxes and showed similar behavior, with little or no Fe incorporation in the nominally Fe-doped layers. This data suggests that the Fe floats on the surface of the growing crystal, concentrating in the liquid Ga droplets and incorporating locally at levels detectable by SIMS once the

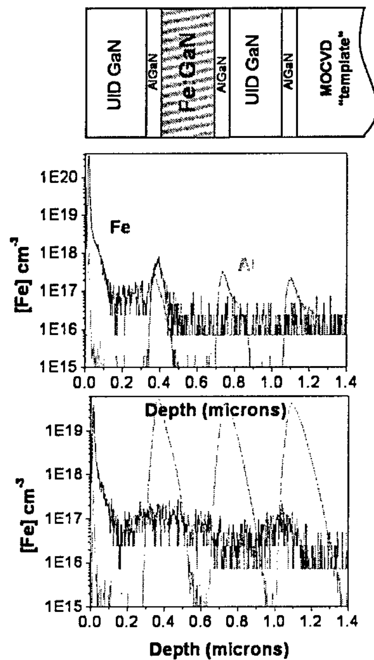

Figure 7 SIMS data from high-intermediate (top) and low-intermediate (bottom) nominally Fe-doped samples.

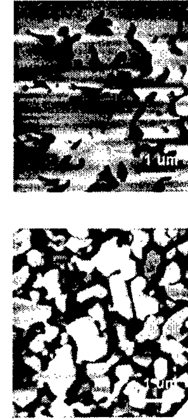

Figure 8 AFM images from high-intermediate (top) and low-intermediate (bottom) nominally Fe-doped samples.

Figure 8 shows AFM images from these samples. The surface morphology was typical for intermediate GaN, with large areas of smooth, pit-free basal plane GaN in between large pits. Though there was some appreciable incorporation in the low intermediate sample, the low levels of the Fe concentration and the spread-out Fe signal suggest that, as in the droplet regime, surface segregation may be significant in the intermediate regime. The presence of a liquid-like Ga adlayer on the surface during intermediate regime growth may be contributing to segregation and preventing Fe incorporation; this is currently being investigated further.

Figure 9 shows SIMS data from three samples grown in the N-rich growth regime for various Fe cell temperatures. All three show clear Fe incorporation in the nominally Fe-doped layer, with mean Fe concentrations increasing with Fe cell temperature. Figure 10 is a plot of the natural log of Fe concentration in the Fe-doped layer as a function of the inverse Fe cell temperature. This yields a linear relationship with a slope corresponding to an activation energy of 3.51 eV, which agrees well with a literature value for the heat of sublimation of Fe of 4.13 eV [Smithell's Metals Reference Book, 6th ed., Butterworths, 1983]. The fact that the Fe incorporates under N-rich conditions, where there is no presence of excess Ga on the sample

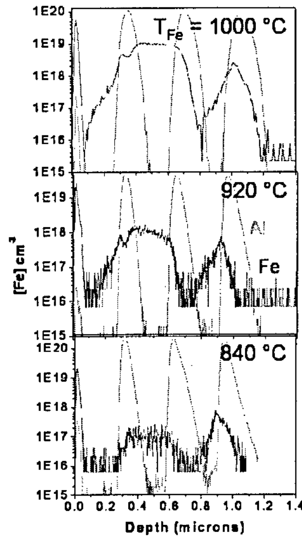

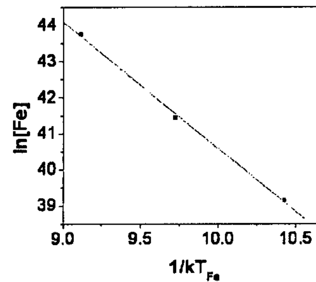

Figure 9 SIMS data from N-rich samples grown at various Fe cell temperatures.

Figure 10 Linear relationship between ln[Fe] and $1/kT_{Fe}$.

In addition to clear Fe incorporation in the nominally-doped layer, the SIMS data for all three samples show an anomalous Fe peak at the MOCVD/MBE regrowth interface. While it is unclear what caused this peak, we suspect that some Fe had deposited on the sample before the growth was started. This theory is currently under investigation.

Figure 11 shows cross-sectional TEM images taken from a sample with three Fe-doped layers sandwiched between UID GaN layers grown in the N-rich regime. Thin (~25 nm) InGaN layers were used as markers in this sample between the Fe-doped and UID layers. The images reveal threading dislocations which propagate from the template into the material, as well as some planar defects that nucleate in the Fe-doped layers. The planar defects are invisible for g= 0002 and visible for g=$1\bar{1}00$, while partial dislocations bounding them are visible for g= (0002). The planar defects which propagate along the [0001] direction seem to "fold" into planar defects in the basal plane, which are most likely basal stacking faults. These defects could be inversion domain boundaries, but due to the presence of bounding partial dislocations, seem more like to be prismatic stacking faults. In addition, it appears that there may be a thin second phase layer near the sample surface, which could be related to segregation during growth. Further TEM is necessary to determine the nature of this layer and of the planar defects and their relation to basal stacking faults and partial dislocations; this work is currently underway.

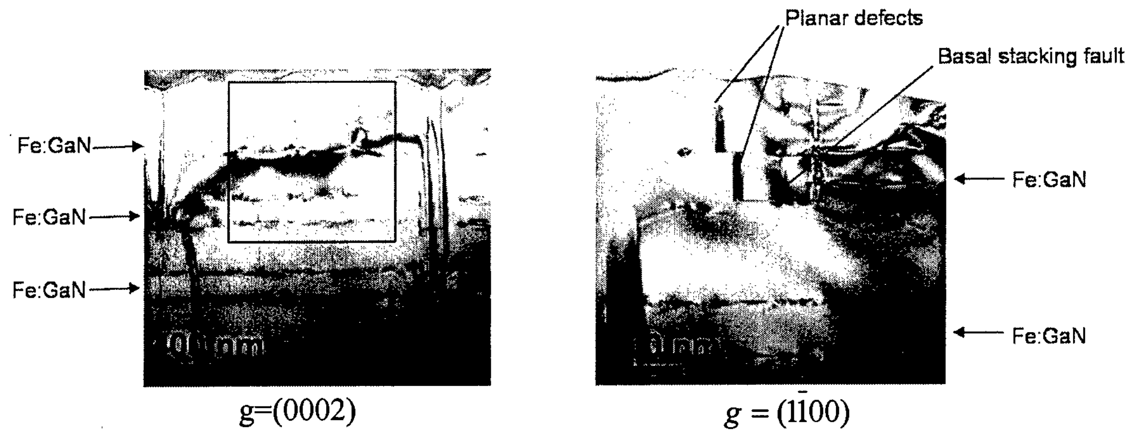

Figure 11 BF TEM images from a N-rich sample with three Fe-doped layers. The box in the g= (0002) image illustrates the region shown in the $g = (1\bar{1}00)$ image.

The results of CV measurements are shown in Fig. 12. All three samples were grown under N-rich growth conditions; two were Fe-doped at approximately 10^{17} and 10^{18} cm^{-3}, and the third was a UID control sample. The samples all show a large increase in charge at the MBE/MOCVD interface, and there is no clear trend of carrier concentration with increasing Fe doping. Further electrical measurements, including Hall measurements, are currently underway in order to determine the compensation activity of the Fe in the material.

We conclude that for rf-plasma MBE, incorporation of transition metals (Fe in this case) is challenging under Ga-rich conditions. We have been successful in Fe incorporation under the more compromised N-rich growth conditions.

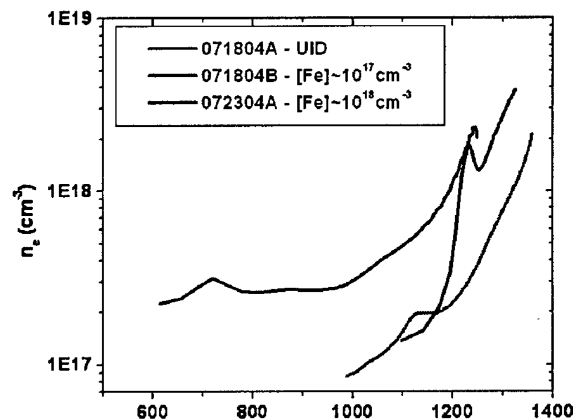

Appendix I

Sddharth Rajan, Arpan Chakraborty, Umesh K. Mishra, Christian Poblenz, Patrick Waltereit, and James S. Speck, " MBE Grown AlGaN/GaN HEMTs on SiC," *Int'l. J. High Speed Electron. Sys.*, submitted for publication.

International Journal of High Speed Electronics and Systems
© World Scientific Publishing Company

MBE-Grown AlGaN/GaN HEMTs on SiC

SIDDHARTH RAJAN*, ARPAN CHAKRABORTY AND UMESH K. MISHRA
Electrical and Computer Engineering Department, University of California, Santa Barbara, Santa Barbara CA 93106, USA

CHRISTIANE POBLENZ, PATRICK WALTEREIT AND JAMES S. SPECK
Materials Department, University of California, Santa Barbara, Santa Barbara CA 93106, USA

We report on the development of AlGaN/GaN high-electron mobility transistors (HEMTs) grown on SiC using plasma-assisted molecular beam epitaxy (MBE). In this work, we show that performance comparable to state-of-the-art AlGaN/GaN HEMTs can be achieved using MBE-grown material. Buffer leakage was an important limiting factor for these devices. The use of either carbon-doped buffers, or low Al/N ratio in the nucleation layer growth were effective in reducing buffer leakage. Studies varying the thickness and concentration of the carbon doping were carried out to determine the effect of different carbon doping profiles on the insulating and dispersive properties of buffers. On devices without field plates, at 4 GHz an output power density of 12 W/mm was obtained with a power-added efficiency (PAE) of 46 % and gain of 14 dB. 15.6 W/mm with PAE of 56 % was obtained from these devices after field-plating. Two-tone linearity measurements of these devices were also carried out. At a C/I3 level of 30 dBc, the devices measured had an output power of 1.9 W/mm with a PAE of 53 %. The effect of the Al/N ratio in the AlN nucleation layer on buffer leakage was studied. N-rich conditions yielded highly insulating GaN buffers without carbon doping. At 4 GHz, devices without field plates delivered 4.8 W/mm with a PAE of 62 %. At a higher drain bias (50 V), 8.1 W/mm with a PAE of 38 % was achieved.

Keywords: Gallium Nitride; HEMT; microwave; carbon; MBE

1. Introduction

We report on our work on AlGaN/GaN HEMTs grown by plasma-assisted MBE on 4H-SiC substrates. MBE HEMTs have recently demonstrated excellent power performance at microwave frequencies[1][2][3][4][5]. In-situ diagnostic techniques, a carbon-free and hydrogen-free growth environment, low source consumption, good interfaces and low point defect density are some of the advantages of MBE growth over MOCVD growth. One of the main issues in AlGaN/GaN HEMTs is obtaining an insulating, non-dispersive buffer. MBE-grown undoped buffers can be conductive unless grown under certain specific conditions.

To reduce the buffer leakage in these devices, we employed two methods. In the first method carbon doping was used to make the buffer insulating. Carbon, however, causes dispersion that degrades device performance.

*e-mail: srajan@ece.ucsb.edu

It was found that moving the 2DEG away from the carbon removed dispersion. The insulating and non-dispersive buffers helped achieve excellent microwave power and linearity performance.

We also explored insulating buffers without the use of carbon doping. AlN nucleation layer growth in N-rich conditions resulted in a GaN buffer with reduced buffer conductivity. Using optimized growth conditions, uniformly insulating buffers were achieved. The devices grown on these buffers demonstrated high power and efficiency.

2. Carbon-doped buffers

The devices in this work were grown on a Varian Gen II MBE system with an rf-plasma nitrogen source. Carbon was introduced using a CBr_4 gas delivery system[6], [7]. All HEMT structures were grown on semi-insulating 4H-SiC substrates from Cree, Inc.

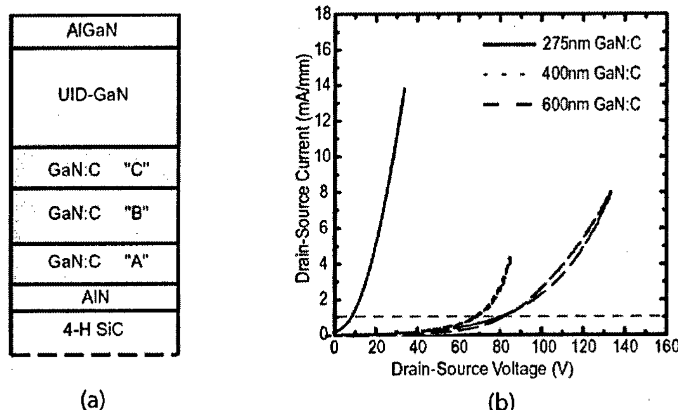

Fig. 1. (a) Epitaxial structure of 1st generation C-doped devices. The thickness of the C-doped layer was 400 nm. (b) Leakage between isolation patterns. The patterns were 3.4 μm apart.

In Fig. 1(a) we show the layer structure of a first-generation C-doped device. A two-step buffer for dislocation reduction was employed [8], [9], [10]. In Fig. 1(b) the leakage from a C-doped samples with a varying C-doped layer thickness is shown. A tapered doping profile was used with carbon doping concentration of $6 \times 10^{17} cm^{-3}$, $4 \times 10^{17} cm^{-3}$, $2 \times 10^{17} cm^{-3}$ in regions A, B, and C, respectively. Leakage between isolation patterns on these structures was studied. The ohmic pads were separated by 3.4 μm. As shown in the figure, it was seen that a higher carbon concentration does increase the insulating property of the buffer. For the doping concentration shown, 400 nm of C-doped GaN was sufficient for an insulating buffer. The distance between the C-doped layer and the 2DEG was 300 nm.

DC and small-signal characterization of these devices was carried out after SiN passivation. A thin SiN layer was grown under the gate before processing to reduce gate leakage. Charge and mobility in these devices were similar to carbon-free samples. A saturated current > 1 A/mm was obtained with a current gain cutoff frequency (f_T) of 20 GHz and unity power gain frequency (f_{MAX}) of 44 GHz. The device had a gate length of 0.7 μm and were 150 μm wide. Large-signal load-pull measurements were carried out on the devices. At 4 GHz, a maximum output power of 4 W/mm with a power-added efficiency (PAE) of 18 % was obtained at a drain bias of 35 V. These values were lower than expected, and large-signal RF-IV measurements were then conducted to investigate the problem. The large signal RF-IVs were measured using a microwave transition analyzer (MTA). As shown in Fig. 2 (a) the large-signal RF-IV showed significant knee walkout. Comparable devices without carbon in the buffer did not exhibit this knee walkout after passivation, and this suggested that the carbon was responsible for the large-signal dispersion.

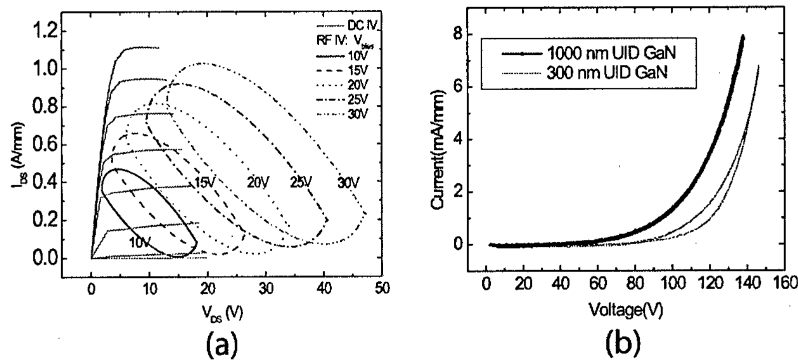

Fig. 2. (a) RF-IV curves at 4 GHz superimposed on the DC IV plot. Significant knee walkout was observed. (b) Leakage between isolation patterns for structures with 300 nm and 1 μm undoped GaN between the 2DEG and the C-doped region

To remove the effect of carbon, the distance between the carbon-doped layer and the 2DEG was increased from 300 nm to 1 μm. However, it was necessary to ensure that the buffer leakage did not increase due to the thicker unintentionally doped (UID) layer. In Fig. 2 (b), the leakage current in the buffer for different thicknesses of the undoped layer between the carbon and the 2DEG is shown. For a UID layer of up to 1 μm, there was no significant increase in the buffer leakage. Devices with this thick UID GaN layer were then tested and RF-IV's on these devices showed that the RF dispersion was reduced. Excellent power and efficiency performance was obtained from these devices. In Fig. 3(a), 4 GHz power data of a device biased at 30 V is shown. The device delivered 5 W/mm with a high PAE of 66 %. At 70 V, the same device delivered 12 W/mm with a PAE of 46 %. To the authors'

knowledge, this is the highest reported power from a SiN-passivated device without field plates on either MBE-grown or MOCVD-grown material.

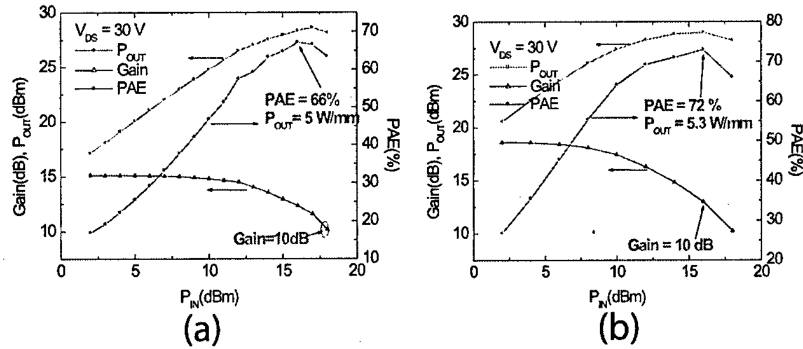

Fig. 3. 4 GHz Power characteristics of MBE-grown AlGaN-GaN HEMTs (a) without field-plate and (b) with field plate.

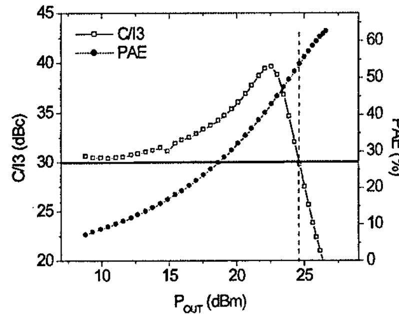

Fig. 4. Two-tone measurement results at 4 GHz. An output power of 1.9 W/mm with a PAE of 53 % was obtained at 4 GHz at a C/I3 level of 30 dBc. The drain bias was 30 V.

The devices were then field-plated [11] by depositing Ni/Au gates above the passivation layer. The field-plate length was 0.7 μm and the overlap with the gate was 0.3 μm. The field-plated devices showed an increase in output power and efficiency. Fig. 3 (b) shows power data for field-plated devices with 4 GHz cw input. The devices delivered an output power of 5.3 W/mm with a PAE of 72 %. At 70 V, the output power was 15.6 W/mm with a PAE of 55 %. This is currently the highest reported power value for MBE-grown AlGaN/GaN devices.

Two-tone measurements on these devices showed that they have excellent linearity characteristics. Results from two-tone measurements with the carrier to in-

termodulation product ratio (C/I3) maintained at greater than 30 dBc are shown in Fig. 4. An output power of 1.9 W/mm with a PAE of 53 % was achieved at a drain bias of 30 V. Measurements for a minimum C/I3 ratio of 45 dBc were also carried out. For a C/I3 greater than 45 dBc, an output power of 1 W/mm with a PAE of 37 % was achieved.

3. Undoped Buffers

MBE-grown buffers are not insulating under all growth conditions. We studied the influence of the nucleation layer growth conditions on the buffer layer conductivity. These growth studies revealed that the presence of Al droplets significantly increased the leakage in the buffer. In Fig. 5(a) we show the current through isolation patterns. GaN buffers with the AlN nucleation layer grown in N-rich conditions were found to be most insulating. More detailed measurements showed that the wafer was uniformly resistive and that the isolation was as good or better than the C-doped samples.

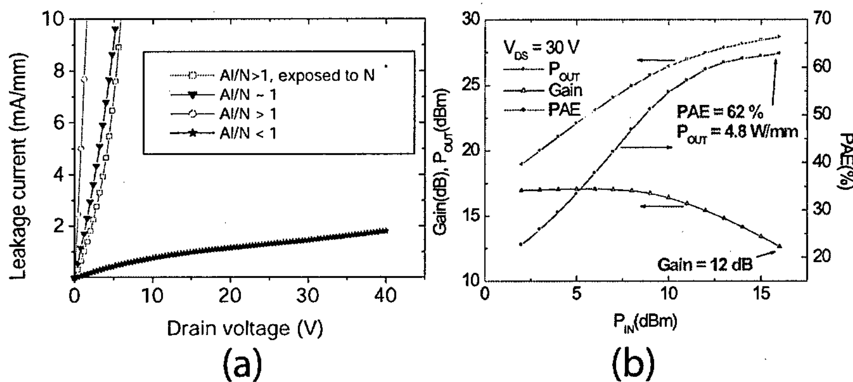

Fig. 5. (a) Comparison of buffer leakage between samples grown under different nucleation conditions. (b) 4 GHz power characteristics of undoped buffer devices.

Devices measured on these buffers had DC and small-signal properties similar to C-doped HEMTs. However, due the absence of a SiN insulating layer under the gate, the gate leakage in these devices was slightly higher than the C-doped devices discussed earlier in the work. In Fig.5(b) we show 4 GHz power measurement data for one of these devices. The device delivered 4.8 W/mm with a PAE of 62 % at a drain bias of 30 V. At a higher drain bias of 50 V, the transistor delivered 8.1 W/mm with a PAE of 38 %. These numbers indicate that undoped MBE buffers can be employed for high performance AlGaN/GaN transistors.

4. Conclusion

Carbon doping was shown to be a reliable and reproducible method to achieve highly insulating and non-dispersive buffers for AlGaN/GaN HEMTs. Excellent power and linearity characteristics were demonstrated in devices with C-doped buffers. Growth and electrical studies of the nucleation layer reveal that employing N-rich conditions during growth of the nucleation layer led to highly insulation buffers. Devices on these buffers had excellent DC and microwave properties.

Acknowledgments

We would like to acknowledge financial support from DARPA (Program Manager Edgar Martinez) managed by ONR (Contract Monitor Harry Dietrich) and from the AFOSR (Program Manager Gerald Witt).

References

1. J. S. Moon, M. Micovic, P. Janke, P. Hashimoto, W.-S. Wong, R. D. Widman, L. McCray, A. Kurdoghlian, and C. Nguyen, "GaN/AlGaN HEMTs operating at 20GHz with a continuous-wave power density >6W/mm," *Electronics Letters*, vol. 37, p. 528, 2001.
2. D. S. Katzer and S. C. Binari and D. F. Storm and J. A. Roussos and B. V. Shanabrook and E. R. Glaser, "MBE growth of AlGaN/GaN HEMTs with high power density," *Electronics Letters*, vol. 38, p. 1740, 2002.
3. N. G. Weimann, M. J. Manfra, and T. Wächtler, "Unpassivated AlGaN-GaN HEMTs with Minimal RF Dispersion Grown by Plasma-Assisted MBE on Semi-Insulating 6H-SiC Substrates," *IEEE Electron Device Letters*, vol. 24, p. 57, 2003.
4. R. Behtash, H. Tobler, M. Neuburger, A. Schurr, H. Leier, Y. Cordier, F. Semond, F. Natali, and J. Massies, "AlGaN/GaN HEMTs on Si(111) with 6.6W/mm output power density," *Electronics Letters*, vol. 39, p. 626, 2003.
5. S. Rajan, P. Waltereit, C. Poblenz, A. Chakraborty, S. J. Heikman, J, S, Speck, and U. K. Mishra, "Power Performance of AlGaN/GaN HEMTs grown on SiC by Plasma-Assisted MBE", *IEEE Electron Dewice Letters*, vol. 25(5), p. 247, 2004.
6. D. S. Green, J. S. Speck, and U. K. Mishra, "CBr_4 doping of GaN in rf plasma MBE," *J. App. Phys.*, vol 95, p. 8456, 2004.
7. C. Poblenz, P. Waltereit, S. Rajan, U. K. Mishra, and J. S. Speck, "Effect of carbon doping on buffer leakage in AlGaN/GaN high electron mobility transistors , " *J.Vac.Sc.Tech. B*, vol. 22, p. 1145, 2004.
8. B. Heying, X. H. Wu, S. Keller, Y. Li, D. Kapolnek, B. P. Keller, S. P. DenBaars, and J. S. Speck, "Control of GaN surface morphologies using plasma-assisted molecular beam epitaxy," *Appl. Phys. Lett.*, vol. 68, p. 643, 1996.
9. M. J. Manfra, N. G. Weimann, J. W. P. Hsu, L. N. Pfeiffer, and K. W. West, "Dislocation and morphology control during molecular-beam epitaxy of AlGaN/GaN heterostructures directly on sapphire substrates," *Appl. Phys. Lett.*, vol. 81, p. 1456, 2002.
10. P. Waltereit, C. Poblenz, S. Rajan, U. K. Mishra, and J. S. Speck, "Growth of GaN buffer layers on 4H-SiC(0001) by plasma assisted molecular beam epitaxy for high mobility electron transistors ," *Appl. Phys. Lett.*, submitted for publication.
11. A. Chini, D. Buttari, R. Coffie, L. Shen, S. Heikman, A. Charaborty, S. Keller, U. K. Mishra, "Power and linearity characteristics of field-plated recessed-gate AlGaN-GaN HEMTs," *IEEE Electron Device Letters*, vol. 25(5), p. 229, May 2004.